



The influence of the crevice induced IR drop on polarization measurement of localized corrosion behavior of 316L stainless steel

E. Shojaei, M. Mirjalili, M.H. Moayed*

Materials and Metallurgical Engineering Department, Faculty of Engineering, Ferdowsi University of Mashhad, Mashhad 91775-1111, Iran

ARTICLE INFO

Keywords:

A. Stainless steel
B. Polarization
C. Crevice corrosion
Galvanostatic
SEM

ABSTRACT

This paper evaluates the role of *IR* drop on initiation of the crevice corrosion of 316 L stainless steel in 3.5% NaCl solution. For this purpose, potentiodynamic and galvanostatic experiments and macroscopic/microscopic observations were implemented at crevice gaps of 30, 60, 120 and 240 μm . According to the results, two distinct stages of crevice corrosion of 316 L stainless steel were observed: crevice initiation and propagation. The crevice corrosion was found to be initiated by scattered pits without any significant *IR* drop. However, when the current increased due to pitting occurrence, the *IR* drop increased considerably.

1. Introduction

The occluded geometry of a crevice separates anodic and cathodic locations of corrosion circuits. Therefore, the current flowing through the electrolyte resistance between the anodic site in the occluded environment of crevice and the cathodic site at the outer surface, produces an *IR* drop which is associated with a potential difference between the interior and exterior regions of the crevice [1–3]. In other words, *IR* drop refers to the amount of potential drop which is obtainable by multiplication of the current and the resistance of the electrolyte existing in the crevice [4].

The *IR* drop mechanism was first proposed by Pickering [3,4], who believed that crevice corrosion occurs only when the magnitude of *IR* drop is large enough to shift the potential of anodic site to active state. In other words, crevice corrosion occurs by transition of the potential from passive to the active state, when the *IR* exceeds a critical value (*IR**). *IR** is the difference between the applied potential on the crevice outer surface and the active-to-passive transition potential [5].

According to the *IR* drop mechanism, the *IR* causes the electrode potential to shift to active values at regions located beyond a critical distance from the crevice mouth [3,4]. The critical distance is defined as a certain distance within the crevice, where the potential drops to values lower than the passive-to-active potential and thus crevice corrosion takes place. It should be noted that this critical distance could be affected by active-to-passive potential of material, crevice geometry, passive current density, applied potential at the surface outside the crevice, and solution conductivity. It has been indicated that a narrow crevice gap provides a smaller critical distance [6]. Moreover, a higher

passive current density and a lower solution conductivity cause a decrease in the value of critical distance. In addition, it has also been evidenced that *IR* drop significantly increases under the above-mentioned conditions [7].

It is reported that when the crevice corrosion develops stably, there will be a significant *IR* drop established due to accumulation of rust at the crevice opening. It has been also claimed that acidification and accumulation of the chloride ion in the occluded crevice geometry extend the potential range of active corrosion [8]. However, other results showed that chloride ions promote the crevice corrosion by increasing the *IR* value, as chloride increases the corrosion current [7]. In addition, the facts that current and resistance respectively increase due to acidification and accumulation of corrosion products, have been explained in terms of an *IR* drop mechanism [9].

Another factor, which could affect the *IR* drop, is crevice geometry. It has been reported that the *IR* drop decreases by increasing crevice width and by reducing the crevice depth. For example, while the potential drop for crevice width of 10 μm could be 500 mV, its value could become negligible when the crevice width is increased to 1000 μm . Moreover, the potential drop of a crevice could vary from 0.65 mV to 5000 mV, when its depth is shifted from 0.1 cm to 10 cm. Quantitative comparison of the results indicated that the potential drop in crevice solution is more sensitive to crevice depth than crevice width [10]. It has been inferred that the depth/gap ratio of a crevice geometry affects the potential drop [11].

Chang et al. [11] employed a 316 L stainless steel to simulate the initiation stage of crevice corrosion in 1 M NaCl and 3.5% NaCl solutions. The results of the simulation indicated that the potential drop

* Corresponding author.

E-mail address: mhmoayed@um.ac.ir (M.H. Moayed).

<https://doi.org/10.1016/j.corsci.2019.04.030>

Received 5 June 2018; Received in revised form 23 April 2019; Accepted 24 April 2019

Available online 09 May 2019

0010-938X/ © 2019 Elsevier Ltd. All rights reserved.

inside a crevice consists of two components: the chemical potential drop, and the physical potential drop. The chemical potential drop is calculated just by considering chemical changes of the ionic species and mass transfer. However, the physical potential drop is created by the viscosity of the solution or the geometrical resistance of the crevice, etc. It was reported that at the end of the initiation time of crevice corrosion, the chemical potential drop from the crevice mouth to its bottom was about 20 mV. Nevertheless, the total potential drop seemed to be 4–10 times larger due to the physical IR drop.

It has been asserted that increase in IR drop is usually associated with initiation of active corrosion within the crevice. There were also some evidences, showing that IR drop has promoted propagation of crevice corrosion [12,13]. Shaw et al. [8] investigated the role of ohmic potential drop on the initiation of crevice corrosion of alloy 625 in seawater. They calculated an IR drop of approximately 300 mV, which caused the metal within the crevice to reside at a potential in the active nose of the anodic polarization curve, resulting in transpiring of metal's active dissolution. Therefore, it was revealed that the IR drop plays an important role in initiation of crevice corrosion. In addition, once initiated, crevice corrosion propagation is maintained by the IR drop at the bottom of the crevice. However, other scholars believed that an initiation mechanism, which is only based on IR drop, is insufficient to explain the initiation of crevice corrosion in stainless steels, which have very strong passivity. In other words, the potential shift mechanisms by IR drop in the crevice solution need to be supported by the effect of chemical reactions in the crevice solution [10].

The aim of this study is to investigate the effect of IR drop on initiation and propagation of the crevice corrosion of 316 L stainless steel. The influence of crevice gap on the magnitude of the IR drop is also discussed by studying crevice gaps of 30, 60, 120, and 240 μm .

2. Experimental procedures

2.1. Materials and preparation

Chemical composition of the 316 L stainless steel used in this work is listed in Table 1. The alloy was cut into rods with cross-sectional areas of 0.78 cm^2 . In order to prevent occurrence of unwanted crevice corrosion at the specimen/epoxy interface, all specimens were primarily pre-passivated in 0.1 M Na_2SO_4 solution [14]. Pre-passivation of the specimens was implemented by applying a constant anodic potential of 900 mV (SCE) to the specimens for 20 min. The specimens were then mounted in an epoxy resin. Prior to each experiment, the working electrode surface was manually wet-ground using 60–1200 grit silicon carbide papers. All electrochemical measurements were carried out in 3.5 wt. % NaCl solutions and using a Gill AC automated potentiostat (ACM instruments). The solutions were prepared using deionized water and analytical grade of sodium chloride. All experiments were conducted at room temperature of $25 \pm 2^\circ\text{C}$.

2.2. Crevice preparation procedure

An artificial crevice with constant width and length of 10 and 32.5 ± 2.5 mm, respectively, was made on the surface of specimen by using a glass plate and an inert transparent foil (cling film) for spacing. It should be noted that the electrochemical experiments were carried out for crevice gaps of 30, 60, 120, and 240 μm using different thickness of cling film. The edges of the glass plate were sealed with bees wax and colophony mixture. Before immersion, the crevice hole was filled with

Table 1
Chemical composition of the studied 316 L stainless steel (wt.%).

Cr	Ni	Mn	C	Si	Mo	P	S	Fe
18.599	10.037	1.727	0.007	0.299	2.02	0.030	0.014	Bal.

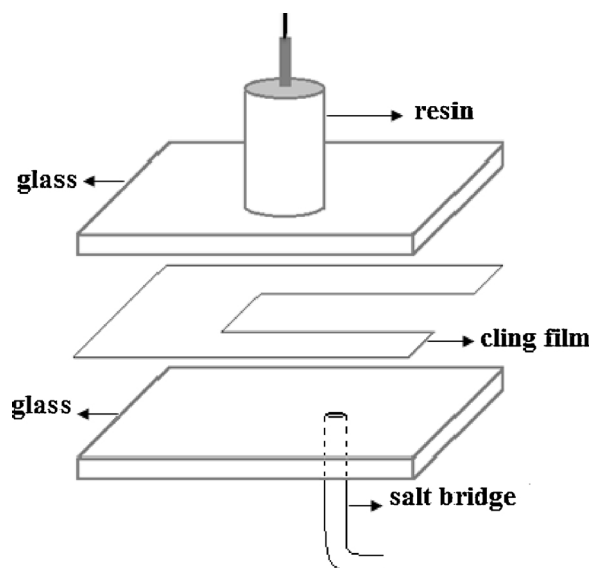


Fig. 1. Schematic of the crevice setup showing the geometry of the crevice formed by an inert foil and the location of the salt bridge's tip near the specimen inside the crevice.

electrolyte using a squeeze bottle in order to eliminate air bubbles. In order to calculate the IR drop in this study, the internal and external potentials of crevice were measured separately by using a cell with two distinct reference electrodes. A saturated KCl-agar salt bridge tube, which had been electrochemically connected to a saturated calomel electrode (SCE), was used as a reference electrode for measurement of internal potential of the crevice. The length and diameter of agar salt bridge were 10 cm and 3.5 mm, respectively. The tip of the salt bridge tube was located close to the specimen inside the crevice. A schematic of the setup is illustrated in Fig. 1.

2.3. Electrochemical cell

Electrochemical setup included a four-electrode cell consisting of working, counter, and two reference electrodes. Two SCEs were utilized to measure internal and external potentials of the crevice. Platinum foil was also used as counter electrode. The cell arrangement for performing the experiments with its equivalent electrical circuit is shown in Fig. 2. The internal and external potentials of the crevice were independently measured using two Gill AC automated potentiostats (ACM instruments).

Ignoring capacitance related current, the polarization resistance (R_p) between the specimen and the salt bridge connected to the internal reference electrode (RE_1) in passivity region is given by Eq. (1):

$$R_p = R_{ct} \quad (1)$$

where R_{ct} is the charge transfer resistance on the surface of the crevice specimen. However, after the probable occurrence of pitting on the surface of crevice specimen, the polarization resistance (R_p) is obtained by Eq.(2):

$$R_p = R_{ct} + R_{pit} \quad (2)$$

where R_{ct} is the charge transfer resistance in the pit cavity, and R_{pit} is the resistance of the solution inside the pit, when a pit is formed on the surface of the crevice.

However, the total resistance (R_{total}) between the specimen and the external reference electrode (RE_2) can be calculated by using Eq. (3):

$$R_{total} = R_p + R_{crevice} + R_s \quad (3)$$

where $R_{crevice}$ is the resistance of the crevice electrolyte located between the specimen and crevice mouth and R_s is the bulk solution

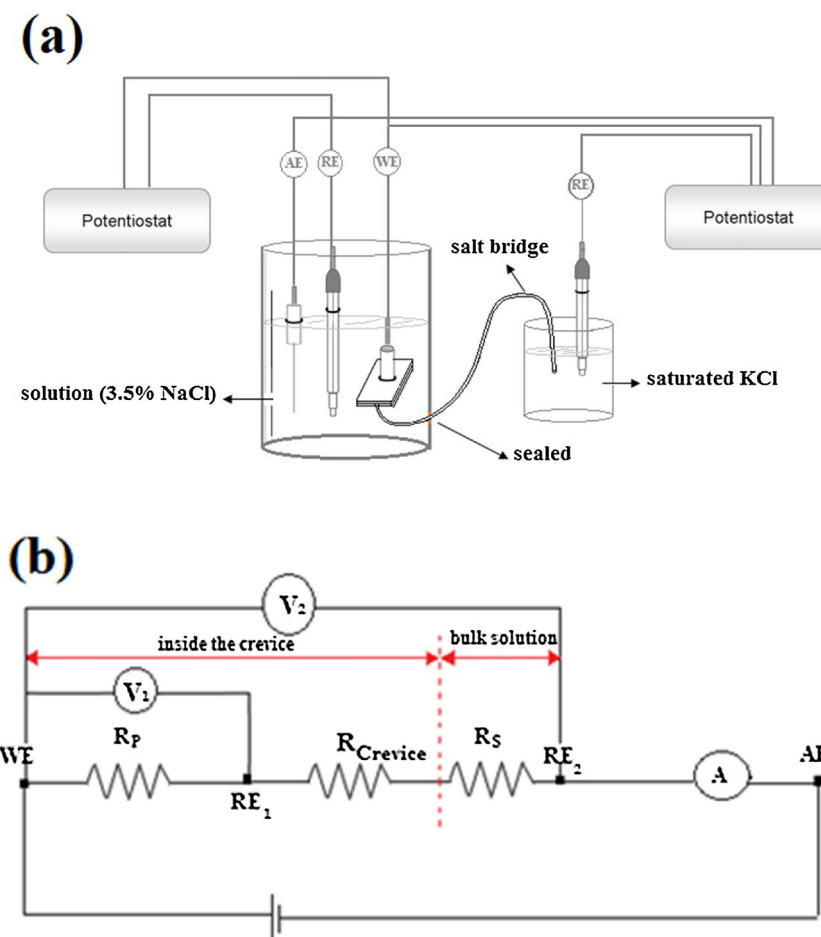


Fig. 2. Electrochemical cell: (a) the cell arrangement for crevice corrosion experiments, (b) cell's equivalent electrical circuit.

resistance. According to Fig. 2, and Eqs. (1–3), the IR drop associated with the crevice geometry ($IR_{crevice}$) is obtained from the potential difference between the two reference electrodes (ΔV_1 and ΔV_2), considering the following equations:

$$\Delta V_1 = IR_p \quad (4)$$

$$\Delta V_2 = I(R_p + R_{crevice} + R_s) \quad (5)$$

Ignoring the solution resistance (R_s) for simplification, as its value is relatively low; Eq. (6) renders $IR_{crevice}$, as follows:

$$IR_{crevice} = \Delta V_2 - \Delta V_1 \quad (6)$$

2.4. Potentiodynamic experiments

Potentiodynamic polarization measurements were carried out using the internal reference electrode by sweeping the working electrode potential from the rest potential up to 650 mV (SCE) at a given scan rate ($1 \text{ mV} \cdot \text{min}^{-1}$). The current density of $3 \text{ mA} \cdot \text{cm}^{-2}$ was considered as the maximum current density for stopping the polarization. For all experiments, the polarization was started after 60 min recording the specimen's corrosion potential in the solution. This rest period was enough for the specimen to reach a steady state condition. Simultaneously, the external reference electrode was used to measure the external potential of the crevice. For each crevice gap, the experiments were repeated 3 times to validate the reproducibility and reliability.

2.5. Galvanostatic experiments

Galvanostatic experiments were used to evaluate the role of IR drop on initiation and propagation of the crevice corrosion. The polarization was carried out using the internal reference electrode and by applying the constant current density of $5 \mu\text{A} \cdot \text{cm}^{-2}$ in the four-electrode cell. The second external reference electrode was simultaneously used for measuring the external potential of the crevice. Before the examination, open circuit potential was measured for 900 s. The resulting potential fluctuations of the applied galvanostatic current were monitored for 10 h. The experiments were repeated 3 times at the crevice gaps of 30 and 60 μm .

2.6. Characterization of surface morphology

Potentiodynamic polarizations were also used to characterize the crevice corrosion damage. To this end, the samples were brought out of the experimental setup at different times with distinct values of potential drop. The samples' surfaces were then subjected to an ultrasonic bath for removing the covers, which have been possibly formed on the probable pits. They were then kept in a desiccator to reduce the possibility of air oxidation and electrode contamination prior to surface analysis. Subsequently, morphological characterization of the electrode surfaces was performed by means of several equipment including optical microscope (OLYMPUS BX60 M), stereomicroscope (OLYMPUS SZX9), and scanning electron microscopy (LEO 1450, Germany) with energy dispersive X-ray spectroscopy (EDS).

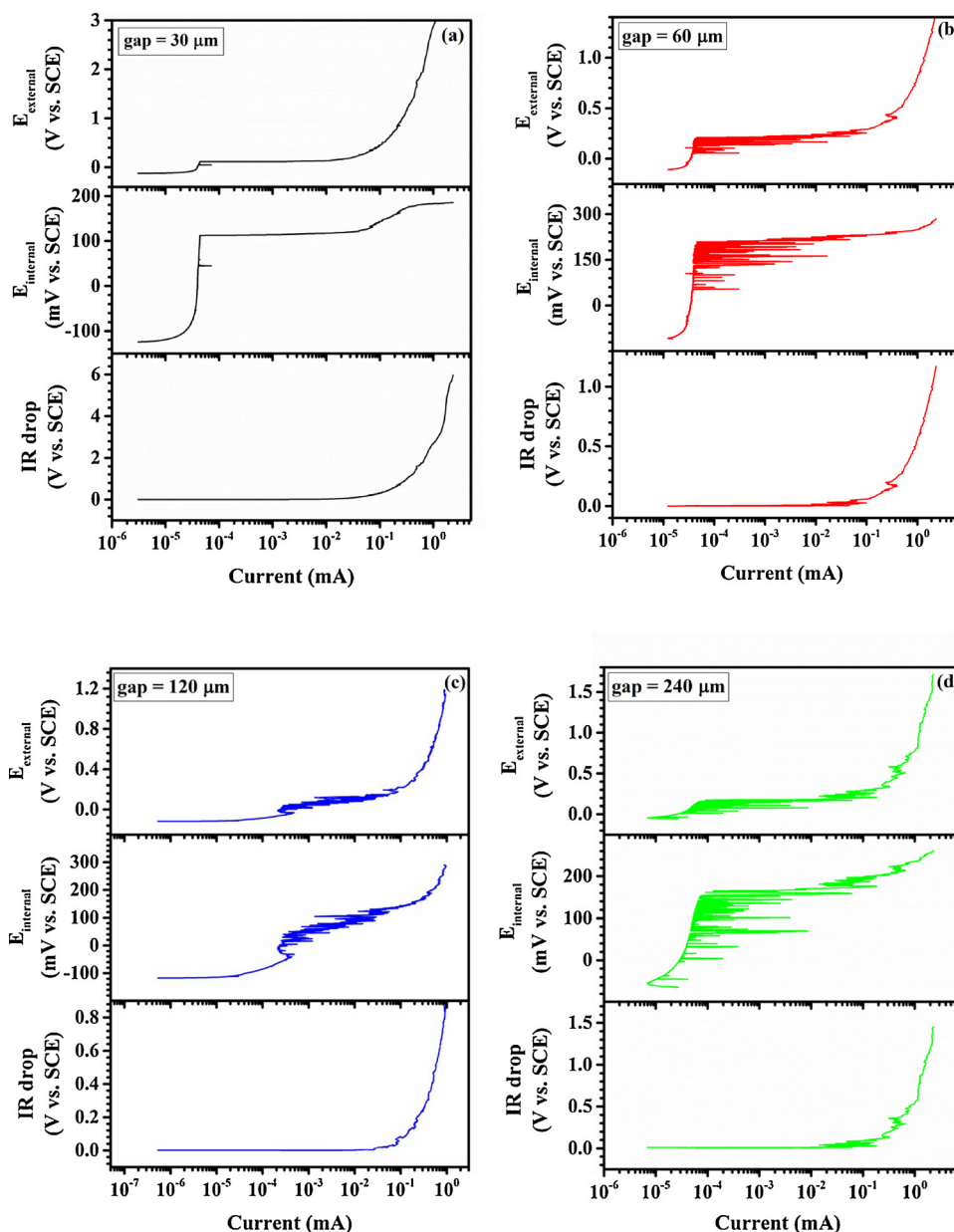


Fig. 3. The anodic potentiodynamic polarization plots of 316 L stainless steel consisting of three curves of external potential-current, internal potential-current, and IR drop-current: (a) crevice gap of 30 μm, (b) crevice gap of 60 μm, (c) crevice gap of 120 μm, (d) crevice gap of 240 μm.

3. Results

3.1. IR drop in potentiodynamic experiments

The anodic polarization plots of 316 L stainless steel with crevice gaps of 30, 60, 120 and 240 μm are illustrated in Fig. 3. They consist of three curves of external potential-current, internal potential-current, and IR drop-current. As can be seen, the potentiodynamic behavior shows a passive region and a breakdown potential due to pitting. Comparison of external and internal potentials of the crevices indicates that in the region of passivity, the measured potentials are nearly the same. However, the increment of IR drop is observable at the time when the current increases, especially after pitting corrosion occurrence. In other words, the IR drop curves consist of two parts: 1) during passive state, 2) after stabilization of the pitting corrosion. IR drop is insignificant during the passive state; however, it increases to considerable values by increasing the current in the second part. Fig. 4 compares how the potential drops (IR) of the specimens having different crevice

gaps vary by the current. It can be said that the potential drop increases with the current linearly; the slope of this linear relationship could be used to estimate the crevice electrolyte resistance (R_{crevice}). It is evident that the potential drop declines with increasing the size of the crevice gap. The values of the crevice electrolyte resistance (R_{crevice}) versus the reciprocal crevice gap (d) have been represented in Fig. 4, which shows a linear behavior. The figure shows that R_{crevice} increases by decreasing the crevice gap thickness (d).

3.2. IR drop in galvanostatic experiments

For better understanding, the IR drop was evaluated by galvanostatic experiments at the crevice gaps of 30 and 60 μm. It should be noted that these geometries could provide conditions that are more critical rather than the gaps of 120 and 240 μm. Based on Fig. 5a and b, it can be said that at galvanostatically applied current density of 5 μA.cm⁻², crevice corrosion was successfully initiated and propagated on the surface. As can be seen, stable crevice corrosion was initiated

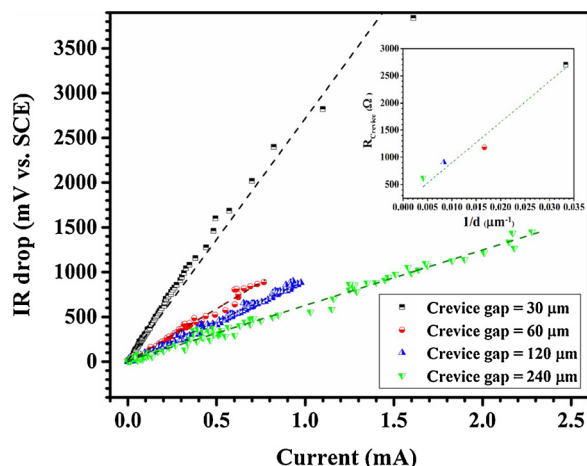


Fig. 4. The linear relationship between IR drop and current at different crevice gaps. The slop of the fitted line can be regarded as the crevice electrolyte resistance. The internal curve shows $R_p \cdot \frac{1}{d}$ relationship.

when the specimen potential dropped suddenly (dashed-line). However, it was reported that the potential of the specimen has remained approximately constant during the galvanostatic experiments when no crevice existed [15]. Moreover, it is evident that the difference between the internal and external potentials is insignificant. Based on this figure, the maximum potential drops within the crevice gaps of 30 and 60 μm were approximately 10 mV (SCE). Comparing the galvanostatic curves in Fig. 5 reveals that by decreasing the crevice gap size from 60 μm to 30 μm, the potential drop increases.

3.3. Surface morphology

As mentioned earlier, according to the IR drop theory, crevice corrosion is expected to be happen at a critical distance from the crevice opening [3–7,16,17]. However, the theory of stabilization of metastable pits claims that the pit initiation sites, which are randomly distributed on the specimen's surface, are the preferred sites for initiation of crevice corrosion [18]. Hence, for investigation of crevice corrosion mechanism of 316 L stainless steel, surface of samples was studied by stereomicroscope, optical microscope and scanning electron microscope. For this purpose, specimens were brought out of the experimental setup of potentiodynamic polarization at two different potential drop ranges: (a) small IR drops (potential drops lower than 100 mV) and (b) significant IR drops (potential drops more than 1000 mV).

Fig. 6 illustrates images of the sample's surface when the IR drop was insignificant during the potentiodynamic experiments. The crevice bottom is on the right side in all of the images. As can be seen, the first observable signs of destruction on the crevice specimen have been appeared in form of stable pits scattered on the surface; Distribution of the formed pits does not follow a certain pattern with distance from the crevice opening. Fig. 6e shows a pit in the initial stage of breakdown. As can be seen, the surrounding area of the pit is etched.

After breakdown potential and increasing of the current, the IR drop has increased considerably. Fig. 7a shows the image of destructed surface of the sample after a significant increase in the IR drop. Fig. 7b illustrates SEM image of a stable pit on the surface close to the crevice opening; however, the density of pits in this region was relatively low. Fig. 7c and d depict the destructed surfaces located in the crevice's central area and in regions close to the crevice bottom, respectively. As indicated in Fig. 7a, regions close to the crevice bottom are more susceptible to pitting due to more acidic environment and accumulation of aggressive solution. It should be noted that white arrows indicate the crevice bottom direction in all images.

Optical microscopy images shown in Fig. 8 compare the sample

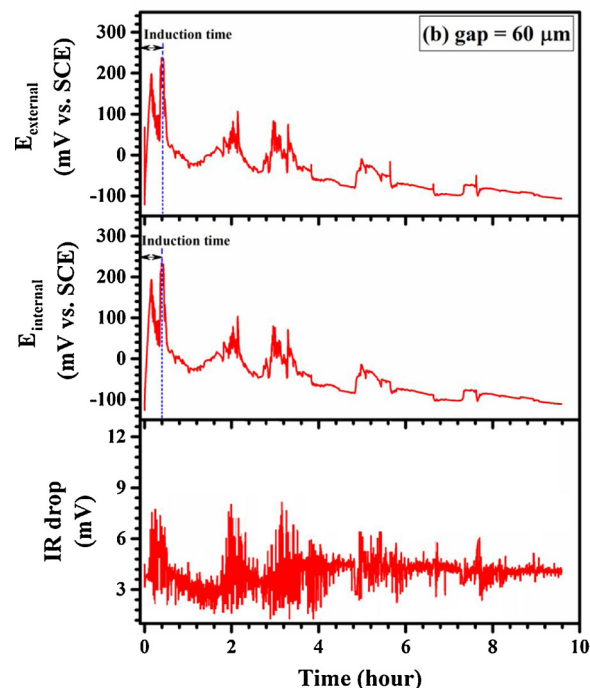
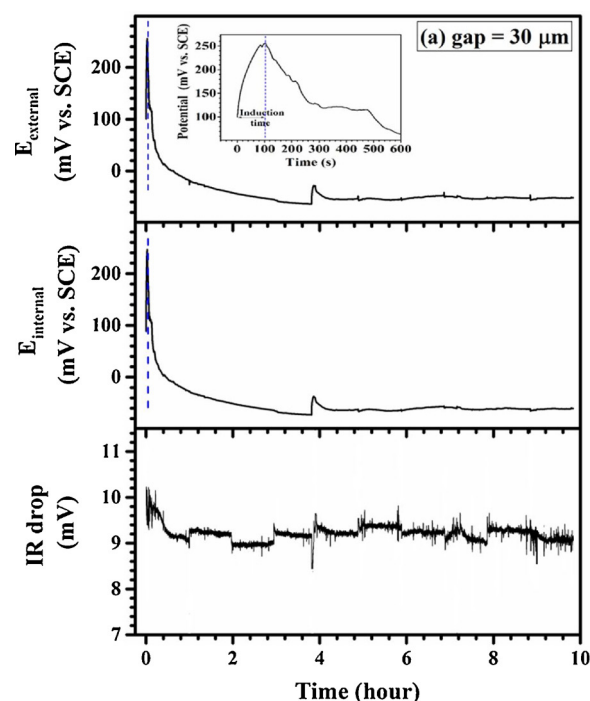


Fig. 5. Potential-time behavior of 316 L stainless steel in 3.5% NaCl solution when an anodic current of $5 \mu\text{A}\cdot\text{cm}^{-2}$ is galvanostatically applied to the electrode: (a) crevice gap of 30 μm, (b) crevice gap of 60 μm.

destruction after galvanostatic experiments in three regions: (a) at a surface close to the crevice opening, (b) in the central area of the specimen, and (c) at a surface close to the crevice bottom. The big white arrows in these images indicate the direction towards the crevice bottom and the small ones point out the pits. As can be seen, tiny pits are randomly distributed over the surface inside the crevice.

The pit nucleation sites were characterized by a SEM microscope equipped by EDS. Fig. 9a indicates SEM image of an inclusion as a pit

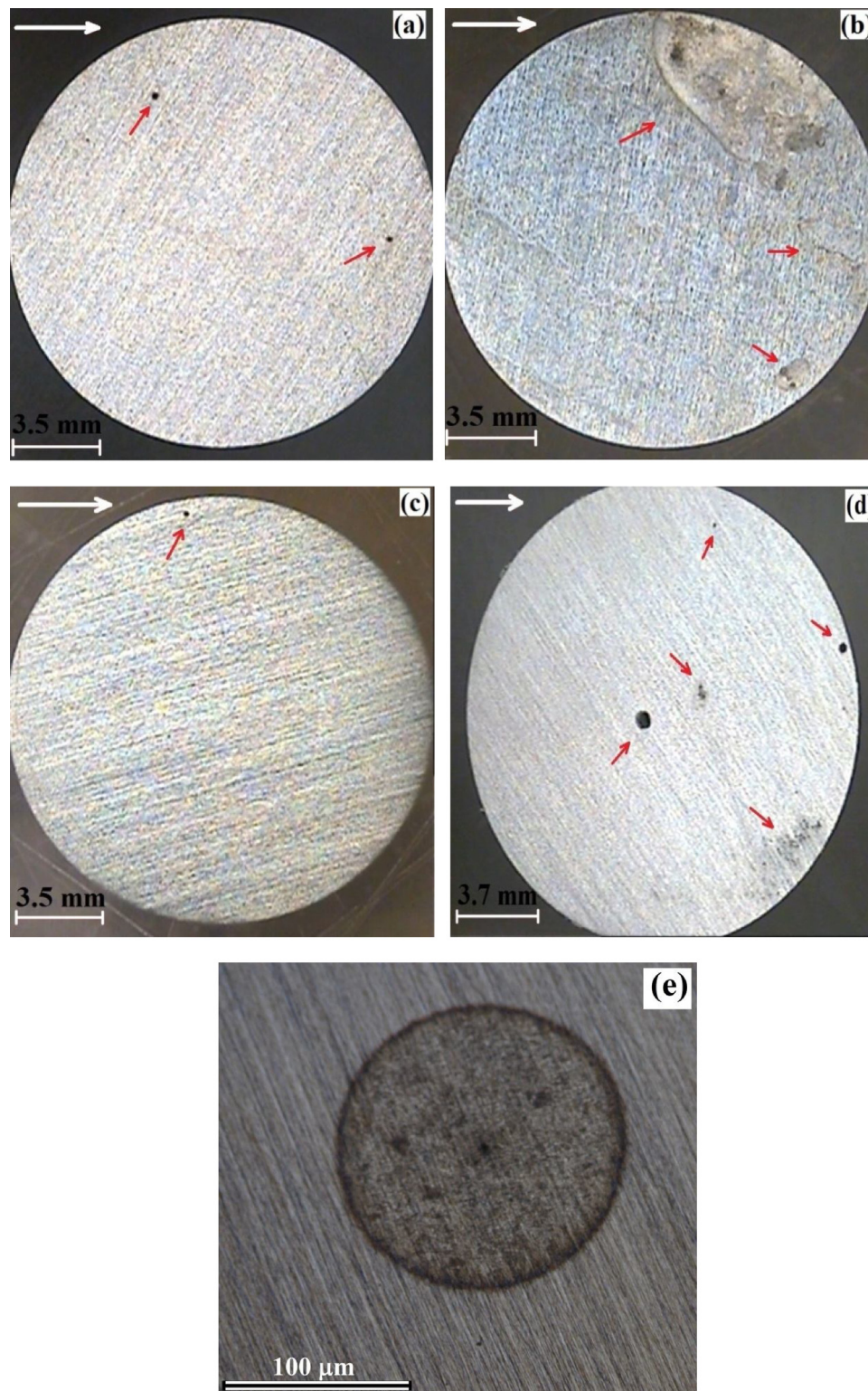


Fig. 6. Stereomicrographs of the crevice specimens when IR drop was small in potentiodynamic experiments: (a) crevice gap of 30 μm , (b) crevice gap of 60 μm , (c) crevice gap of 120 μm , (d) crevice gap of 240 μm . (e) Optical microscopy image of a pit showing etched surface in the surrounding area.

initiation site. As seen in Fig. 9b, the EDS analysis implies that the pits have mostly nucleated on MnS inclusions.

4. Discussion

4.1. The influence of the IR drop on corrosion behavior of 316 L stainless steel

By considering Figs. 6–9, it is figured out that the crevice corrosion has been initiated by stabilization of metastable pits inside the crevice.

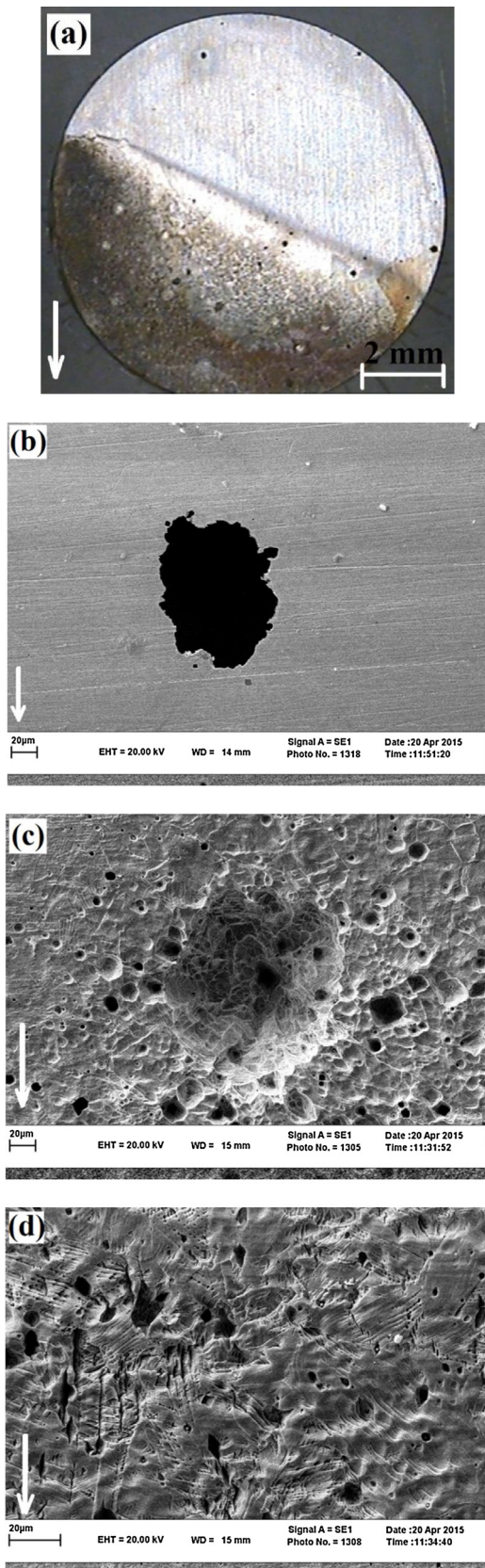


Fig. 7. Stereomicrographs and SEM images of the crevice specimen when IR drop was significant in potentiodynamic experiments: (a) photograph image of corroded surface of specimen, (b) SEM image of the surface close to the crevice opening, (c) SEM image of the central area of the specimen, (d) SEM image of the surface close to the crevice bottom.

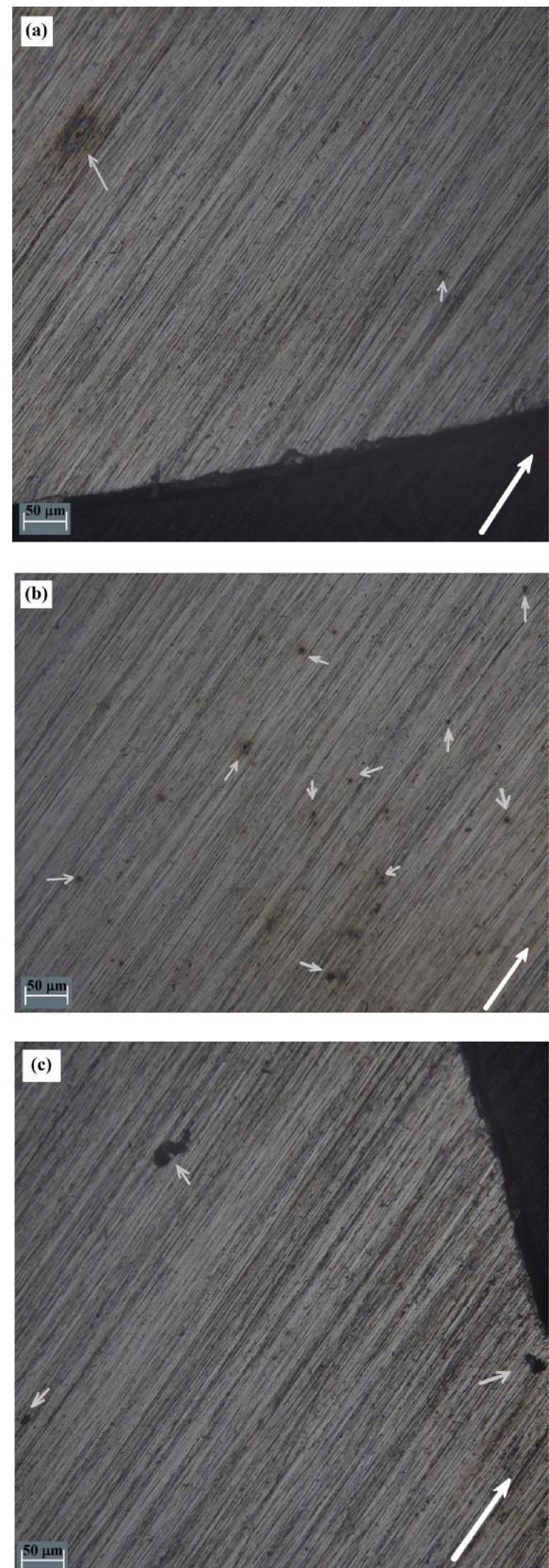


Fig. 8. Optical microscopy images which show the sample's destruction after galvanostatic experiments: (a) at a surface close to the crevice opening, (b) in the central area of the specimen, (c) at a surface close to the crevice bottom.

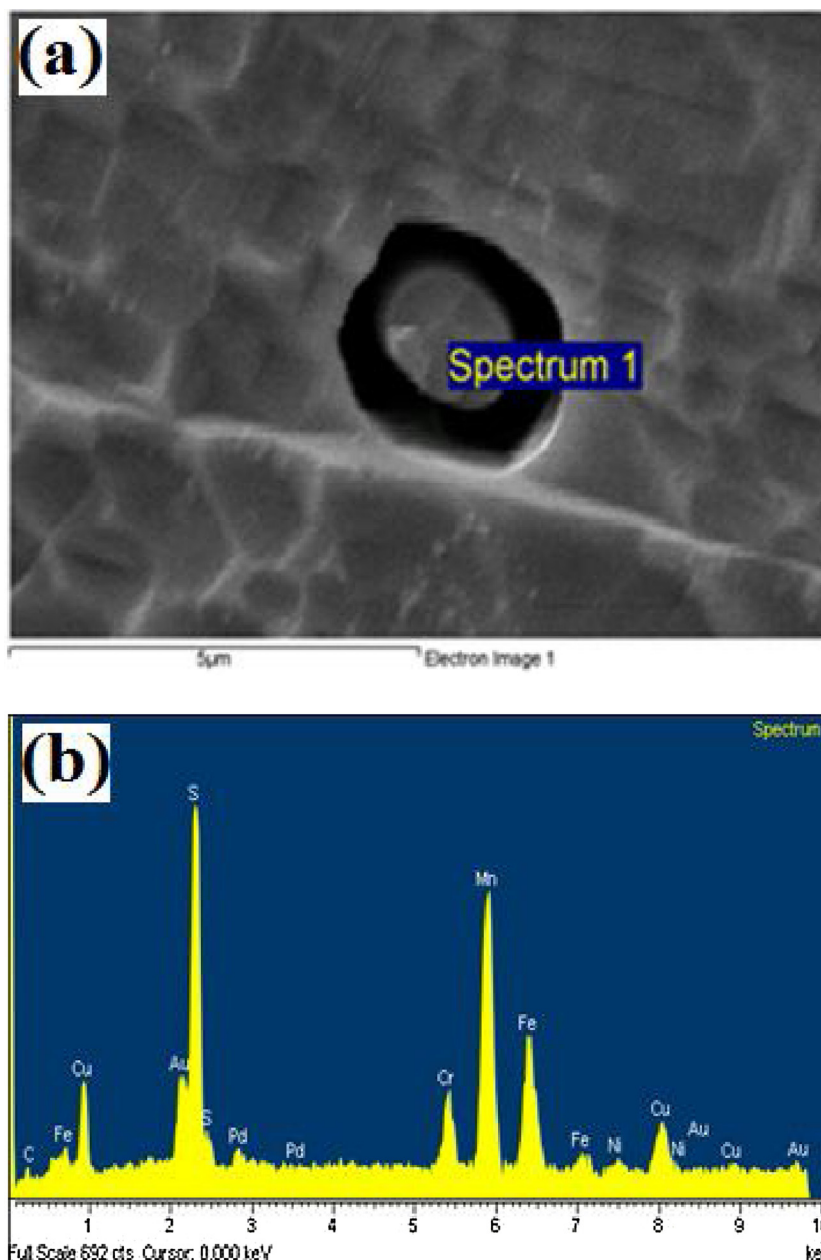


Fig. 9. (a) Scanning electron microscopy (SEM) of the sulphide inclusion as a pit initiation sit, (b) EDS analysis of the MnS inclusion.

Fig. 6e shows a pit with its etched surrounding area. It is an indication of the fact that etching and complete destruction of the surface in crevice corrosion of 316 L initiates from pits. Figs. 6 and 7 compare the morphology of the corroded surface at the initial and latter stages of breakdown, when the pits have initially appeared (Fig. 6) and then led to etching and destruction of the surrounding area (Fig. 7). Accumulation of the cations released by the formation of initial pits leads to a decrease in pH of the electrolyte solution in surrounding area. It yields more pitting and more decrease in pH, until pH is low enough to etch and destruct the surface. It was previously indicated that in the incubation period of the crevice corrosion of stainless steel, the pH inside the crevice gradually decreased from 3.0 to ca. 2.0, and the Cl^- concentration increased from 0.01 to ca. 0.18 M. Moreover, it was shown that generation of the micro-pits led to a sharp decrease in pH to below 0.5 and an increase in the Cl^- concentration to above 4 M [19].

The results of potentiodynamic experiments indicated that IR drop at the initial stage of the breakdown is insignificant, when the pit formation occurred inside the crevice (Fig. 3). Moreover, Fig. 6 shows the

initial signs of crevice corrosion that have appeared in form of pits, while IR drop is still small. Therefore, beginning of the crevice corrosion of 316 L has not been influenced by IR drop value.

These experiments were aimed to show that beginning of crevice corrosion of 316 L, which appears initially by pits, is not influenced by IR drop value. As shown in Fig. 6, the initial signs of crevice corrosion have been appeared in form of pits, while IR drop is still small.

According to the IR drop theory, the ohmic potential drop is dependent to parameters such as current, conductivity and crevice geometry. Its value is given by Eq. (7) [20,21]:

$$IR = \frac{x_{pass} I}{\sigma w t} \quad (7)$$

where IR is the potential drop (in mV), x_{pass} is the distance between the crevice mouth and the active-passive boundary inside the crevice (in cm), I is the current (in mA), σ is the conductivity (in $\Omega^{-1} \cdot \text{cm}^{-1}$), w is the crevice width (in cm), and t is the crevice gap thickness (in cm). Based on this equation, IR drop is only affected by the current when

crevice geometry and crevice electrolyte's conductivity are constant. Therefore, when the current is negligible (especially before pitting in the potentiodynamic experiments or at low current densities in the galvanostatic polarizations), the IR drop is not considerable and hence cannot influence the potential and consequently the corrosion rate. In fact, the negligible values of IR drop measured in this study (less than 20 mV) were not sufficient for transition from passive-to-active condition. According to the literature [22], the active-to-passive transition potential for 316 L stainless steel is about -300 mV (vs. SCE); thus, in our study at least an IR drop of 150 mV was needed to enable the active surface corrosion inside the crevice. In agreement with this finding, the maximum IR drop measured by White et al. [12] for the passive current density of 10^{-2} A. m⁻², was about 90 mV which was not enough for surface activation. Furthermore, Alavi and Cottis [23] have also reported that the crevice potentials of 304 SS were 35–50 mV more negative than the external potential, depending on the distance from the crevice mouth at the beginning of ZRA experiment. These values were decreased (to 6–9 mV) at the end of the experiment.

Moreover, studies on Ni-Cr-Mo alloy [24] and Ni-Cr-Mo-W alloy-22 [25] have shown that potential drop occurs after an induction time during the galvanostatic experiments. Authors believed that this potential drop, which corresponded to beginning of the crevice corrosion, was due to activation of some locations within creviced area. According to this theory, the activation stage represents a period, which is required for establishment of a sufficiently large IR drop and creation of critical crevice solution. However, the results of galvanostatic experiments in our study showed that IR drop during the induction time is negligible. In fact, the induction time was required in order to stabilize the pits within crevice.

Taking all these results into account, it can be concluded that IR drop had not an effective role on the initiation of pitting inside the crevice. However, it can be deduced that by a significant increase in the corrosion current, which is caused by formation of pits inside the occluded region, a remarkable increase in the IR drop is observed.

According to the results (Fig. 9), it was found that the preferred sites for pits nucleation are MnS inclusions, which are randomly distributed over the sample surface. These observations are in agreement with previous studies on stainless steels [26], which indicated that manganese sulfide inclusions are the active sites for pitting initiation on the passivated surface stainless steels. These inclusions are randomly distributed over the surface of commercial stainless steel [27–31].

It has been reported that for a constant chloride concentration, initiation of the pitting corrosion occurs when the potential of the pitting sites exceeds the pitting potential [32]. Moreover, it was found that the pitting potential strongly depends on type, size, shape, and coherence of the inclusions existing in the alloy [31,33–36]. Indeed, the pit initiation on the small MnS inclusions occurs at higher potentials compared to the case of large inclusions [37]. In other words, the pitting potential increases by decreasing the size of the inclusions. As seen, distribution of the pits over the surface does not follow a pattern with distance from the crevice opening, whilst higher distances can provide higher IR drops. Thus, it can be concluded that the pit initiation is mostly affected by the size of the inclusions and not by the IR drop. Therefore, when the potential exceeds the localized pitting potential, the pitting occurs.

According to Figs. 3,4, and 7, by increasing the potential during potentiodynamic experiments, the current has increased and subsequently a significant IR drop has established. As a result, etching and complete destruction of the sample's surface have occurred in the direction towards the crevice bottom. The significant increase in the current creates considerable amount of metal cations in the occluded crevice environment. According to our results, the accumulation of the cations released by the formation of primary pits and aggressive anions at the crevice bottom probably leads to a decrease in pH of the electrolyte solution [19]. On the other hand, acidification of the solution due to pitting can cause the surface to be etched, especially when the surface potential drops to active region due to a sufficient IR drop.

Altogether, etching develops on the whole creviced surface until the complete destruction (Fig. 7d). As illustrated in Fig. 7d, pearlite structure has been revealed by surface etching during the polarization. When initial pitting occurs, ions produced and occluded in the crevice change the chemistry of the solution, i.e. pH and aggressive ion concentration. Thus, the passivity condition does not continue which yields to etching and active corrosion. Therefore, IR drop and critical crevice solution could both affect the propagation stage of crevice corrosion; acidification of the occluded solution in the crevice extends the potential range of the active corrosion, and the IR drop decreases the potential to lower values. Thus, the surface potential could lie within the potential range of active corrosion, which is accompanied by complete destruction of the surface.

As quoted in previous studies [38,39], pitting potential of MnS inclusions decreases with decrease in pH of the electrolyte solution within the crevice. Hence, a considerable increase in the number of pits has been observed in the direction towards the crevice bottom. The current finding is in contrast with Pickering et al. [3,4], which believed that pitting occurs only in the regions close to the mouth of the crevice. According to them, since the IR drop in these regions is low the surface undergoes higher potentials, which exceed the pitting potential.

4.2. The influence of crevice gap on the magnitude of IR drop

Comparison of the magnitude of the IR drop for different crevice gaps (Figs. 4 and 5) implies that the crevice electrolyte resistance and subsequently the IR drop will increase by decreasing the gap size. This result is consistent with those reported by Shaw et al. [8] and Heppner et al. [40], which showed that when there is a tight crevice, the value of the ohmic potential drop will be significant.

The crevice electrolyte resistance ($R_{crevice}$) is dependent to the crevice dimensions and the resistivity of the solution [41], as shown by Eq. 8:

$$R_{crevice} = \rho \left(\frac{L}{A} \right) \quad (8)$$

where ρ is the electrolyte resistivity (in Ω .cm), L is the length of the crevice (in cm), and A is the crevice cross-sectional area (in cm²). Hence, according to Eqs. 7 and 8, it can be concluded that the crevice geometry has a considerable effect on the magnitudes of the crevice electrolyte resistance and the potential drop [1,8,21]. In other words, when crevice length and crevice width are constant, increasing the crevice gap reduces the resistance of the solution inside the crevice and subsequently IR drop.

5. Conclusion

According to the results obtained in this paper, which are in line with our other work, crevice corrosion of 316 L stainless steel in 3.5% NaCl is initiated by formation and propagation of pits. Moreover, it was observed that the values of potential drops in the primary stage of crevice corrosion were negligible. Thus, it can be deduced at this stage, the crevice induced IR drop is not an affecting factor in occurrence of the pitting and initiation of the crevice corrosion of 316 L stainless steel. However, it was found that increase of the current after the pit formation, significantly increases the IR drop and as well intensifies the acidification of the crevice solution. Therefore, IR drop and critical crevice solution could both affect the propagation stage of crevice corrosion; acidification of the occluded solution in the crevice extends the potential range of the active corrosion, and the IR drop decreases the potential to lower values. Thus, the surface potential could lie within the potential range of active corrosion, which is accompanied by complete destruction of the surface. Furthermore, increasing the crevice gap reduces the crevice electrolyte resistance and subsequently the IR drop within the crevice.

Data availability

The raw/processed data required to reproduce these findings cannot be shared at this time due to technical or time limitations.

Acknowledgements

This work was performed under the sponsorship of the Ferdowsi University of Mashhad for postgraduate students. Authors gratefully acknowledge Sohrab Pahlavan for his helps.

References

- [1] B. De Force, H. Pickering, A clearer view of how crevice corrosion occurs, *JOM J. Miner. Met. Mater. Soc.* 47 (1995) 22–27.
- [2] A.M. Al-Zahrani, H.W. Pickering, IR voltage switch in delayed crevice corrosion and active peak formation detected using a repassivation-type scan, *Electrochim. Acta* 50 (2005) 3420–3435.
- [3] H.W. Pickering, The significance of the local electrode potential within pits, crevices and cracks, *Corros. Sci.* 29 (1989) 325–341.
- [4] H.W. Pickering, K. Cho, E. Nystrom, Microscopic and local probe method for studying crevice corrosion and its application to iron and stainless steel, *Corros. Sci.* 35 (1993) 775–783.
- [5] B. Cai, Y. Liu, X. Tian, F. Wang, H. Li, R. Ji, An experimental study of crevice corrosion behaviour of 316L stainless steel in artificial seawater, *Corros. Sci.* 52 (2010) 3235–3242.
- [6] Y. Xu, H.W. Pickering, The initial potential and current distributions of the crevice corrosion process, *J. Electrochem. Soc.* 140 (1993) 658–668.
- [7] K. Cho, H.W. Pickering, The role of chloride ions in the IR & IR* criterion for crevice corrosion in iron, *J. Electrochem. Soc.* 138 (1991) L56–L58.
- [8] B.A. Shaw, P.J. Moran, P.O. Gartland, The role of ohmic potential drop in the initiation of crevice corrosion on alloy 625 in seawater, *Corros. Sci.* 32 (1991) 707–719.
- [9] N. Sridhar, D.S. Dunn, Effect of applied potential on changes in solution chemistry inside crevices on type 304L stainless steel and alloy 825, *Corrosion* 50 (1994) 857–872.
- [10] H.-Y. Chang, Y.-S. Park, W.-S. Hwang, A study on the modeling of parameters affecting the Ir drop mechanism in the initiation stage of crevice corrosion, *Met. Mater.* 6 (2000) 505–511.
- [11] H.-Y. Chang, Y.-S. Park, W.-S. Hwang, Initiation modeling of crevice corrosion in 316L stainless steels, *J. Mater. Process. Technol.* 103 (2000) 206–217, [https://doi.org/10.1016/S0924-0136\(00\)00462-3](https://doi.org/10.1016/S0924-0136(00)00462-3).
- [12] S.P. White, G.J. Weir, N.J. Laycock, Calculating chemical concentrations during the initiation of crevice corrosion, *Corros. Sci.* 42 (2000) 605–629.
- [13] H.W. Pickering, R.P. Frankenthal, On the mechanism of localized corrosion of iron and stainless steel I. Electrochemical studies, *J. Electrochem. Soc.* 119 (1972) 1297–1304.
- [14] J. Jun, K. Holguin, G.S. Frankel, Pitting corrosion of very clean type 304 stainless steel, *Corrosion* 70 (2013) 146–155.
- [15] S. Wang, R.C. Newman, Crevice corrosion of type 316L stainless steel in alkaline chloride solutions, *Corrosion* 60 (2004) 448–454.
- [16] G.F. Kennell, R.W. Evitts, K.L. Heppner, A critical crevice solution and IR drop crevice corrosion model, *Corros. Sci.* 50 (2008) 1716–1725.
- [17] Y.Z. Yang, Y.M. Jiang, J. Li, In situ investigation of crevice corrosion on UNS S32101 duplex stainless steel in sodium chloride solution, *Corros. Sci.* 76 (2013) 163–169.
- [18] L. Stockert, H. Boehni, Susceptibility to crevice corrosion and metastable pitting of stainless steels, *Mater. Sci. Forum, Trans. Tech. Publ.* (1991) 313–328.
- [19] M. Nishimoto, J. Ogawa, I. Muto, Y. Sugawara, N. Hara, Simultaneous visualization of pH and Cl⁻ distributions inside the crevice of stainless steel, *Corros. Sci.* 106 (2016) 298–302.
- [20] R.S. Lillard, J.R. Scully, Modeling of the Factors Contributing to the Initiation and Propagation of the Crevice Corrosion of Alloy 625, *J. Electrochem. Soc.* 141 (1994) 3006–3015.
- [21] M.I. Abdulsalam, The role of electrolyte concentration on crevice corrosion of pure nickel, *Mater. Corros.* 58 (2007) 511–513.
- [22] G. Meng, Y. Li, Y. Shao, T. Zhang, Y. Wang, F. Wang, Effect of Cl⁻ on the properties of the passive films formed on 316L stainless steel in acidic solution, *J. Mater. Sci. Technol.* 30 (2014) 253–258.
- [23] A. Alavi, R.A. Cottis, The determination of pH, potential and chloride concentration in corroding crevices on 304 stainless steel and 7475 aluminium alloy, *Corros. Sci.* 27 (1987) 443–451.
- [24] N. Ebrahimi, P. Jakupi, J.J. Noel, D.W. Shoesmith, The Role of Alloying Elements on the Crevice Corrosion Behavior of Ni-Cr-Mo Alloys, *Corrosion* 71 (2015) 1441–1451.
- [25] P. Jakupi, J.J. Noël, D.W. Shoesmith, The evolution of crevice corrosion damage on the Ni-Cr-Mo-W alloy-22 determined by confocal laser scanning microscopy, *Corros. Sci.* 54 (2012) 260–269.
- [26] C. Lemaitre, A.A. Moneim, R. Djoudjou, B. Baroux, G. Beranger, A statistical study of the role of molybdenum in the pitting resistance of stainless steels, *Corros. Sci.* 34 (1993) 1913–1922.
- [27] Y. Tsutsumi, A. Nishikata, T. Tsuru, Pitting corrosion mechanism of Type 304 stainless steel under a droplet of chloride solutions, *Corros. Sci.* 49 (2007) 1394–1407.
- [28] G.T. Burstein, S.P. Mattin, Nucleation of corrosion pits on stainless steel, *Philos. Mag. Lett.* 66 (1992) 127–131.
- [29] R.C. Salvarezza, A.J. Arvia, A. Milchev, Spatial distribution of pits on stainless steel, *Electrochim. Acta* 35 (1990) 289–290.
- [30] M.H. Moayed, N.J. Laycock, R.C. Newman, Dependence of the critical pitting temperature on surface roughness, *Corros. Sci.* 45 (2003) 1203–1216.
- [31] J. Stewart, D.E. Williams, The initiation of pitting corrosion on austenitic stainless steel: on the role and importance of sulphide inclusions, *Corros. Sci.* 33 (1992) 457465–463474.
- [32] V. Hospadaruk, J.V. Petrocelli, The pitting potential of stainless steels in chloride media, *J. Electrochem. Soc.* 113 (1966) 878–883.
- [33] Z. Szklaraska-Śmiałowska, E. Lunarska, The effect of sulfide inclusions on the susceptibility of steels to pitting, stress corrosion cracking and hydrogen embrittlement, *Mater. Corros.* 32 (1981) 478–485.
- [34] Y.S. Lim, J.S. Kim, S.J. Ahn, H.S. Kwon, Y. Katada, The influences of microstructure and nitrogen alloying on pitting corrosion of type 316L and 20 wt.% Mn-substituted type 316L stainless steels, *Corros. Sci.* 43 (2001) 53–68.
- [35] T. Suter, H. Böhni, A new microelectrochemical method to study pit initiation on stainless steels, *Electrochim. Acta* 42 (1997) 3275–3280.
- [36] T. Suter, H. Böhni, Microelectrodes for studies of localized corrosion processes, *Electrochim. Acta* 43 (1998) 2843–2849.
- [37] A. Rossi, B. Elsener, G. Hähner, M. Textor, N.D. Spencer, XPS, AES and ToF-SIMS investigation of surface films and the role of inclusions on pitting corrosion in austenitic stainless steels, *Surf. Interface Anal.* 29 (2000) 460–467.
- [38] A.U. Malik, P.C.M. Kutty, N.A. Siddiqi, I.N. Andijani, S. Ahmed, The influence of pH and chloride concentration on the corrosion behaviour of AISI 316L steel in aqueous solutions, *Corros. Sci.* 33 (1992) 1809–1827.
- [39] K.V.S. Ramana, T. Anita, S. Mandal, S. Kaliappan, H. Shaikh, P.V. Sivaprasad, et al., Effect of different environmental parameters on pitting behavior of AISI type 316L stainless steel: experimental studies and neural network modeling, *Mater. Des.* 30 (2009) 3770–3775.
- [40] K.L. Heppner, R.W. Evitts, J. Postlethwaite, Effect of the crevice gap on the initiation of crevice corrosion in passive metals, *Corrosion* 60 (2004) 718–728.
- [41] M.I. Abdulsalam, H.W. Pickering, The effect of crevice-opening dimension on the stability of crevice corrosion for nickel in sulfuric acid, *J. Electrochem. Soc.* 145 (1998) 2276–2284.